ELSEVIER

Journal of Fluids and Structures 23 (2007) 447–462

JOURNAL OF FLUIDS AND STRUCTURES

www.elsevier.com/locate/jfs

Damping of tubes due to internal two-phase flow

A. Gravelle, A. Ross, M.J. Pettigrew*, N.W. Mureithi

Department of Mechanical Engineering, École Polytechnique, P.O. Box 6079, succ. Centre-Ville, Montréal, Qué., Canada H3T 3A7

Received 30 May 2005; accepted 26 September 2006

Abstract

Two-phase internal flow is present in many piping system components. Although two-phase damping is known to be a significant constituent of the total damping, the energy dissipation mechanisms that govern two-phase damping are not well understood. In this paper, damping of three different clamped–clamped tubes subjected to two-phase air–water internal axial flow is investigated. Experimental data are reported, showing a strong dependence of two-phase damping on void fraction, flow velocity and flow regime. Data-points plotted on two-phase flow pattern maps indicate that damping is greater in a bubbly flow regime. The two-phase damping ratio reaches a maximum value at the highest void fraction before the transition to a churn flow regime. An analytical model that relates the two-phase damping ratio to the interface surface area is proposed. The model is based on rigid spherical bubbles in cubic elementary flow volumes. The analytical results are well correlated with the experiments.

Keywords: Two-phase flow; Damping; Flow parameters; Interface surface area

1. Introduction

Many nuclear and process system components such as heat exchangers and piping elements are subjected to two-phase flows. Two-phase flows may cause severe vibration leading to component failures. To avoid such problems, it is desirable to perform a flow-induced vibration analysis which requires damping information. In the present paper, we propose to study some of the parameters that govern damping of tubes subjected to internal two-phase flow.

Carlucci and Brown (1983) carried out a series of tests on tubes subjected to an axially confined air–water two-phase flow. This experimental study, undertaken on clamped–clamped tubes in annular flow, yielded the following results: damping in two-phase flow is much higher than damping in single-phase flow; damping is strongly dependent on void fraction; fluid velocity of the two-phase mixture seems to have little effect on damping; and confinement plays a significant role.

Thereafter, several researchers have conducted studies on damping, in both axial and cross flow. This work was summarized by Pettigrew and Taylor (2004). The general consensus is that the energy dissipation mechanisms that govern damping in two-phase flow are still not well understood. Therefore, it is desirable to conduct basic tests to identify the governing parameters and to understand the basic energy dissipation mechanisms.

*Corresponding author. Tel.: +1 514 340 4711#45814; fax: +1 514 340 4176.
E-mail address: Michel.Pettigrew@polymtl.ca (M.J. Pettigrew).

0889-9746/$ - see front matter
doi:10.1016/j.jfluidstructs.2006.09.008

Nomenclature

A	area of tube section (m^2)
d	bubble diameter (mm)
D	tube diameter (mm)
E	Young's modulus (GPa)
f_n	natural frequency (Hz)
I	tube second moment of area (mm^4)
L	tube length (m)
m	mass per unit length (kg/m)
N	number of bubbles per unit length of tube
Q	volume flow rate (m^3/s)
S	interface surface area (m^2)
U_{GS}	gas superficial velocity (m/s)
U_{LS}	liquid superficial velocity (m/s)
V	homogeneous flow velocity (m/s)
ε	void fraction
ζ	damping ratio (%)
ρ	mass density (kg/m^3)
σ	surface tension (N/m)

Indices

c	critical
e	outer
g	gas
i	inner
l	liquid
s	structural
v	viscous
f	flow-dependent
2φ	two-phase
t	total

Consequently, simple damping experiments were performed with a single tube subjected to internal air–water flow. Three tubes of similar diameter but of different materials, and hence frequency, were tested over a range of void fractions from 0% (liquid) to 100% (gas) and flow velocities from 1.0 to 5.0 m/s. The results were correlated in terms of two-phase flow regimes. Two-phase damping appears related to the interfacial surface area between the phases.

2. Two-phase flow considerations

2.1. Flow regime

Some knowledge of flow regime is required to understand vibration excitation and damping mechanisms in two-phase flow. Although some attempts were made to define flow regimes, and in particular the transitions between flow regimes quantitatively, recognition and identification of the various regimes is still somewhat subjective. The flow

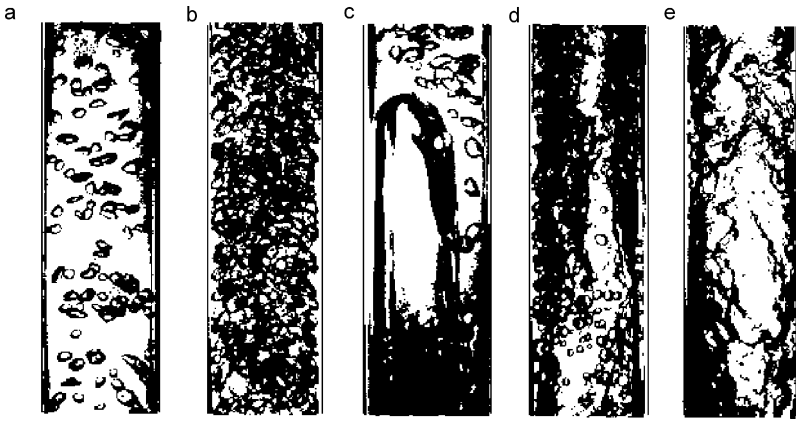

Fig. 1. Flow regimes in air–water ascending flow: (a) bubbly flow; (b) finely dispersed bubbles; (c) slugs; (d) churn; and (e) annular (Roumy, 1969).

patterns shown in Fig. 1 illustrate the most commonly recognized regimes in air–water and steam–water vertical flow (Roumy, 1969). The flow structure belongs to one of the following categories:

(a) *bubbles*: the gas phase is dispersed in relatively large, deformable bubbles that can exist at low velocity flows;
(b) *finely dispersed bubbles*: by increasing the liquid velocity, the gaseous phase breaks down into much smaller bubbles that can generally be considered as rigid spheres;
(c) *slug*: the coalescence of bubbles is forced at larger void fraction and lower liquid flow rate; the gas is thus mainly concentrated in large bubbles (Taylor bubbles) of size close to the tube diameter;
(d) *churn*: at higher flow velocity, the flow pattern becomes much more chaotic; large bubbles of gas constantly break up and reform in a random process;
(e) *annular*: at very high void fraction, the gas fills the core of the tube, and water is confined along the tube wall.

2.2. Homogeneous flow model

Although there is some slip between phases, for simplicity and convenience we assume that the relative velocity between phases in the axial direction can be neglected for the time being. Thus, we can apply the homogeneous model which leads to the following expressions for the two-phase flow parameters. The homogeneous void fraction, ε_g, is defined as the ratio of the gas flow rate to the total flow rate of the two-phase mixture, namely

$$\varepsilon_g = \frac{Q_g}{Q_l + Q_g}, \tag{1}$$

where Q_g and Q_l are the volume flow rates of the gas and liquid phases, respectively. The mixture density ρ is given by

$$\rho = (1 - \varepsilon_g)\rho_l + \varepsilon_g \rho_g, \tag{2}$$

where ρ_g and ρ_l are the densities of the gas and liquid phases. The axial gas and liquid velocities are considered equal, and are given by the homogeneous velocity V defined as

$$V = \frac{\rho_g Q_g + \rho_l Q_l}{\rho A}, \tag{3}$$

where A is the inner cross-section area of the excited tube.

2.3. Two-phase damping

Generally, damping is found to be greater in two-phase mixtures than in single phase flows. Thus, in addition to other damping mechanisms, a two-phase damping mechanism appears to exist due to two-phase flow. This was the point made by Carlucci (1980) when he suggested the following components:

(i) ζ_s: structural damping;
(ii) ζ_v: viscous damping;
(iii) ζ_f: flow-dependent damping; and
(iv) $\zeta_{2\varphi}$: two-phase component of damping.

Hence, the total damping ratio, ζ_t, is given by

$$\zeta_t = \zeta_s + \zeta_v + \zeta_f + \zeta_{2\varphi}. \tag{4}$$

The last component ($\zeta_{2\varphi}$) was introduced to allow for a two-phase component beyond that predicted by single-phase models. Fig. 2, taken from Carlucci (1980), shows the contribution of each component in the total damping, against actual void fraction measurements. Structural damping is not shown on this figure, and is a function of tube material and supports. The two-phase damping $\zeta_{2\varphi}$ (or ζ_{tp}) is dominant over viscous damping ζ_v and flow-dependent damping ζ_f. Two-phase damping also strongly depends on void fraction, whereas viscous and flow-dependent damping is relatively constant. In our tests, described in detail in the next section, we found viscous damping and flow-dependent damping in liquid flow to be very small. This is probably because of internal flow conditions. Thus, viscous damping and flow-dependent damping were ignored, and the two-phase damping in internal two-phase flow is reduced to

$$\zeta_{2\varphi} = \zeta_t - \zeta_s. \tag{5}$$

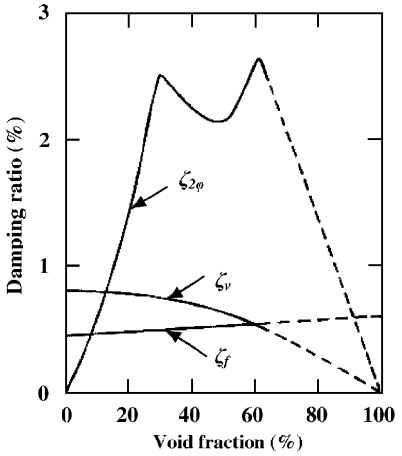

Fig. 2. Damping of a cylinder in confined air–water axial flow (Carlucci, 1980).

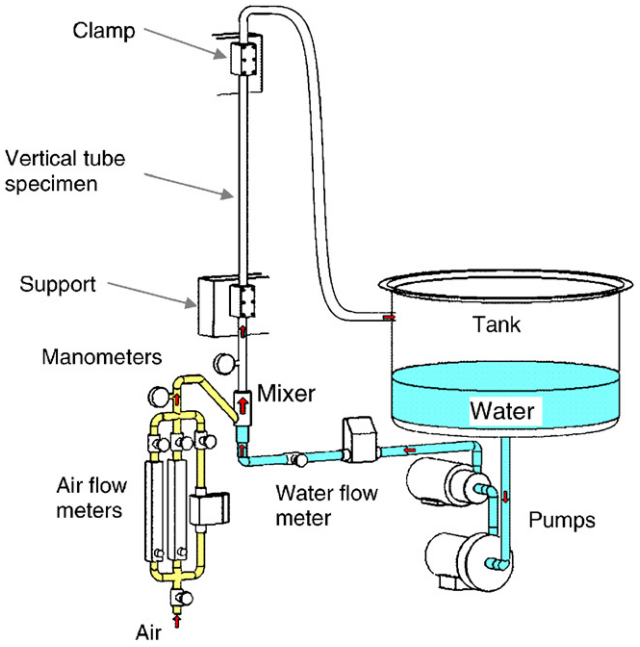

Fig. 3. Test loop.

3. Experimental considerations

3.1. Apparatus

The experimental apparatus consists of a clamped–clamped cylindrical tube subjected to two-phase flow provided by the air–water loop shown in Fig. 3. Water and air are supplied at normal ambient pressure and temperature, and the pre-measured mixture is injected at the bottom of the vertical tube.

A brass tube and two clear polymer tubes (polycarbonate and PVC) were selected for this study. The effective lengths and internal diameters of the tubes were chosen to be similar. Both polymer tubes are very close in mass per unit length, rigidity, and thus natural frequency. The mass per unit length of the brass tube is only about 20% lower than that of the polymer tubes, thus this property is considered similar for all tubes. The rigidity (EI) of the

brass tube is about 3.5 times higher than that of the polymer tubes. Hence, the natural frequency of the brass tube is about twice that of the polycarbonate or PVC tubes. Geometrical and mechanical properties of the test tubes are given in Table 1.

3.2. Experimental procedure

A large number of tests were carried out on each tube, covering the entire range of void fraction (ε_g) and homogeneous flow velocities from $V = 1$ to 5 m/s. Four vibration measurements were performed for each test condition in void fraction increments of 10%.

At the beginning, both the logarithmic decrement and the random vibration techniques were used to measure damping. They were found to give the same results as expected. Since it was faster and simpler, and because of suitable test conditions, the logarithmic decrement technique was then used for most of the tests. The tube was imposed a transverse displacement of 10 mm at mid-length, and released using a quick-release device. The resulting transverse vibration was measured using two pairs of strain gauges. Strain gauges were placed at 90° from each other around the circumference of the tube, near the bottom clamp support where maximum strain occurs. Each strain gauge pair measured the longitudinal deformations in one out of the two orthogonal directions. One pair was used to measure vibrations in the direction given by the excitation device; the second one was used to ensure vibrations were negligible in the other direction.

3.3. Total damping calculation

For each test condition, four free-vibration waveforms were sampled at a frequency of 1000 samples/s. An example of a time response is shown in Fig. 4. The quick-release device is located at mid-span; therefore, the response of the tube is mainly due to the first transverse mode. Because higher order modes do influence the early part of the tube response (shown in Fig. 4), the ten first cycles were discarded from the time record. The logarithmic decrement was then calculated using the waveform peaks as calculation points. The peak amplitude points were plotted on a semi-logarithmic scale, as shown in Fig. 5 for a typical test. Data-points on the semi-log plot were fitted to a straight line from which the slope b was used to determine the damping (Pettigrew and Knowles, 1997):

$$\zeta = \frac{b}{2\pi f_n}, \tag{6}$$

where f_n is the average frequency of oscillation deduced from the logarithmic decrement traces. In all cases, the determination coefficient R^2 (also show in Fig. 5) is very close to unity, indicating that the damping is linear in the amplitude range of interest. In fact, the damping values obtained were repeatable within $\pm 5\%$ of the mean value over the four measurements.

Table 1
General properties of test tubes (*: measured)

Property	Material		
	Brass	Polycarbonate	PVC
Effective length* L (m)	1.45	1.44	1.48
Inner diameter* D_i (mm)	18.0	19.0	21.2
Outer diameter* D_e (mm)	19.0	25.4	26.6
Young's modulus E (GPa)	100	2.3	2.4
Rigidity EI (N m^2)	120	32.2	35.3
Mass per unit length* m (kg/m)	0.254	0.318	0.309
Tube frequency with $\varepsilon_g = 10\%$, $V = 1.5$ m/s* (Hz)	30.1	13.0	14.3
Tube frequency with $\varepsilon_g = 50\%$, $V = 1.5$ m/s* (Hz)	33.6	14.4	15.8
Tube frequency with $\varepsilon_g = 90\%$, $V = 1.5$ m/s* (Hz)	37.0	15.9	17.7
Tube structural frequency in stagnant air* (Hz)	40.8	16	20.2
Structural damping ratio ζ_s in stagnant air (%)	0.07	0.30	0.70

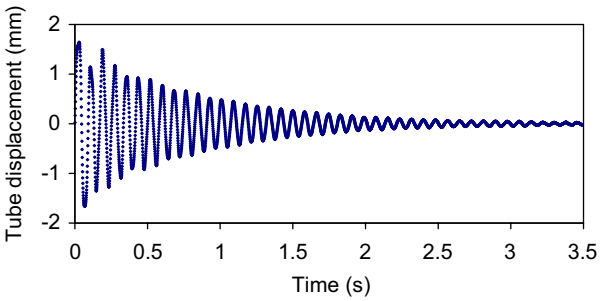

Fig. 4. Typical vibration time-signal as measured on PVC tube.

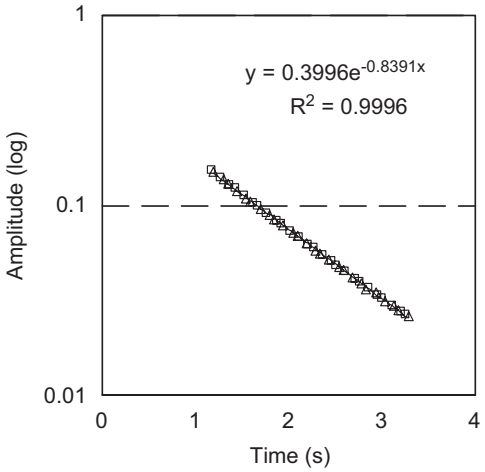

Fig. 5. Peak amplitudes versus time in logarithmic decrement test showing linearity: □ positive peaks; Δ negative peaks. Test data: PVC tube; $\varepsilon_g = 10\%$.

3.4. Two-phase damping

Damping measurements were performed in air to determine the contribution of structural damping (ζ_s) for each tube. The results shown in Table 1 were later used to obtain the two-phase damping component from the experimental data by means of Eq. (5). The structural damping ratios were found to be roughly one order of magnitude lower than the two-phase values. Tests in water ($\varepsilon_g = 0\%$) were also conducted. The measurements are very close to the structural damping measurements, indicating that the effect of liquid flow velocity is negligible, as expected from the theory for clamped–clamped tubes (Païdoussis, 1998).

4. Results and discussion

4.1. Effect of tube frequency

Two-phase damping ratios are generally related to the ratio of fluid forces to inertia forces. This is usually expressed by the term $[\rho D^2/m]$, where ρD^2 and m relate to the fluid forces and the inertia forces, respectively (Pettigrew and Taylor, 2004). Since the values of $[\rho D^2/m]$ are reasonably similar for the three tubes in each test and since the brass tube frequency is approximately twice that of the polymer tubes, it is possible to single out the effect of tube frequency. With added mass due to the fluid, the tube frequency becomes lower, but the frequency ratio between tubes remains similar for all flow conditions, as can be seen in Table 1.

Two-phase damping ratios, $\zeta_{2\varphi}$, are presented with respect to void fraction in Fig. 6(a) and (b) for flow velocities, V, of 5 and 2 m/s, respectively. The trends are similar for all tubes. At the higher flow velocity (Fig. 6(a)), the damping

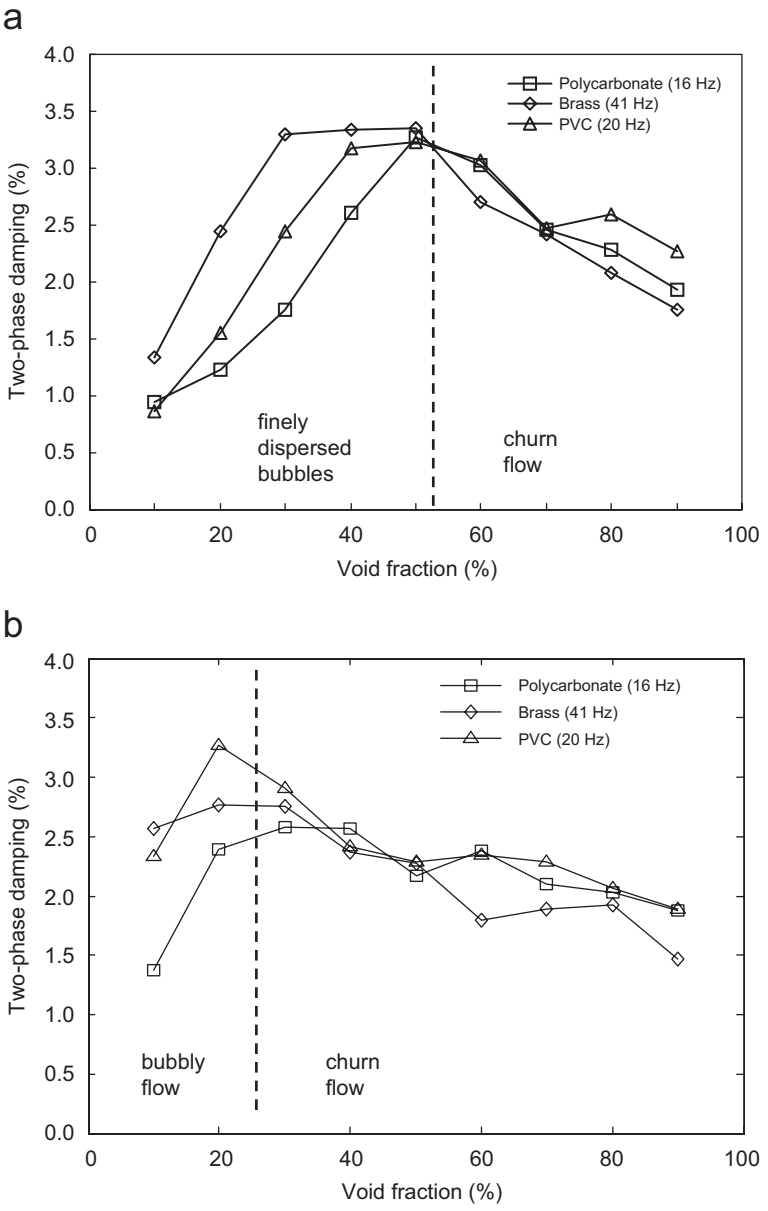

Fig. 6. Two-phase damping for each tube with respect to void fraction: (a) $V = 5\,\mathrm{m/s}$ and (b) $V = 2\,\mathrm{m/s}$.

ratios increase progressively with void fraction, and reach a maximum when the void fraction approaches 50%. Beyond 50%, damping decreases with void fraction. A similar behavior is observed at the lower flow velocity (Fig. 6(b)), except that the maximum is reached at void fractions around 20–40%. It should be noted that the flow regime at low void fractions is either a bubbly flow or finely dispersed bubbles. At high void fractions, the flow regime is churn. For the purpose of completeness, flow regimes are identified, and the boundary between the regimes is superimposed on the graphs (dashed line), based on the Taitel et al. flow maps (discussed in Section 4.3). The graphs show that two-phase damping increases with void fraction in both bubble flows, and it decreases with increasing void fraction in churn flow.

For void fractions above 50%, two-phase damping ratios are very similar for all tubes. At a given flow velocity, the difference between damping ratios is less than 25%. Two-phase damping does not seem to depend much on tube frequency.

For lower void fractions, however, the two-phase damping ratios can vary by a factor of 2 (e.g. 1.7% for polycarbonate and 3.4% for brass when $V = 5\,\text{m/s}$ and $\varepsilon_g = 30\%$). In spite of this, no clear trend with the tube frequency can be found. In fact, both the polycarbonate and PVC tubes have identical frequencies, but their two-phase damping differs as much from one another than they do with the brass tube.

In summary, two-phase damping does not appear to be related to the tube frequency, as expected from earlier work (Carlucci, 1980; Pettigrew and Taylor, 2004). Fluid related parameters are obviously more important. Thus, to understand the fundamental energy dissipation mechanisms, the following discussion will focus on the influence of flow parameters such as void fraction, flow velocity, and flow regime.

4.2. Effects of void fraction and flow velocity

Carlucci (1980) found that because mass flow and void fraction affect flow regime, they have a significant influence on two-phase damping. In light of this observation, a further examination of the effect of flow velocity and void fraction on two-phase damping is proposed. Damping measurements were conducted at various flow velocities and void fractions. Fig. 7 shows the two-phase damping of the PVC tube with respect to void fraction, for flow velocities of 1.5, 2, 4 and 5 m/s. The effect of void fraction is dominant, which is in good agreement with the current literature (Pettigrew and Taylor, 1997; Pettigrew et al., 2001). For any given flow velocity, two-phase damping exhibits similar values and behavior, regardless of the tube specimen. Hence, results are shown and discussed for the PVC tube only.

The effect of void fraction, briefly described above, is expanded here. With increasing void fraction, damping ratios increase to reach a maximum and then decrease in a somewhat irregular fashion. At low void fractions, each damping curve in Fig. 7(a)–(d) is fairly linear. The slopes, $\Delta\zeta_{2\varphi}/\Delta\varepsilon_g$, are in the order of 1% increase in damping ratio for a 10% increase in void fraction. The maximum is reached at void fractions between 20% and 50%.

Damping is significantly affected not only by void fraction but also by flow velocity in a most unexpected way. Although the maximum damping values are quite similar (between 2.9% and 3.5%) for the four different curves of Fig. 7, the void fraction at which the maximum is attained depends on the flow velocity. Table 2 shows the maximum

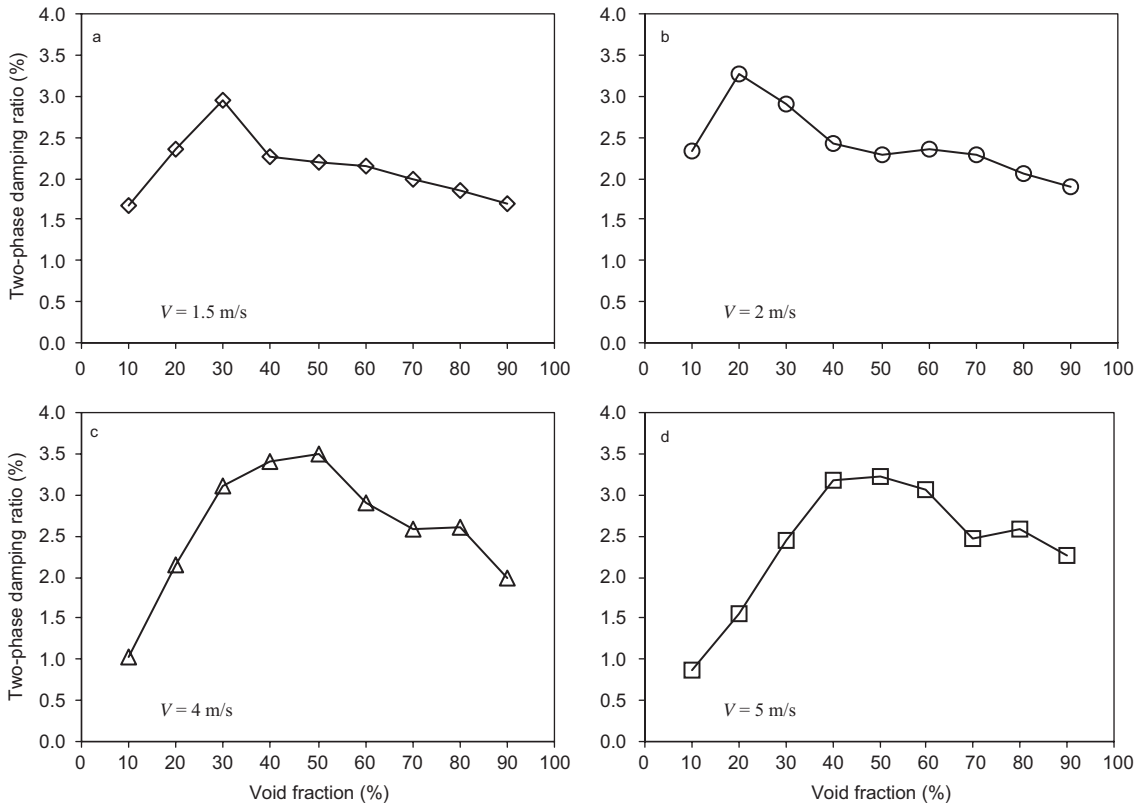

Fig. 7. Effect of void fraction on two-phase damping in PVC tube, for flow velocities of (a) 1.5 m/s, (b) 2 m/s, (c) 4 m/s, and (d) 5 m/s.

Table 2
Maximum two-phase damping and related void fraction, with respect to flow velocity: PVC tube

Velocity (m/s)	$\zeta_{2\varphi max}$ (%)	ε_g at $\zeta_{2\varphi max}$ (%)
1.5	2.94	30
2	3.27	20
4	3.50	50
5	3.22	50

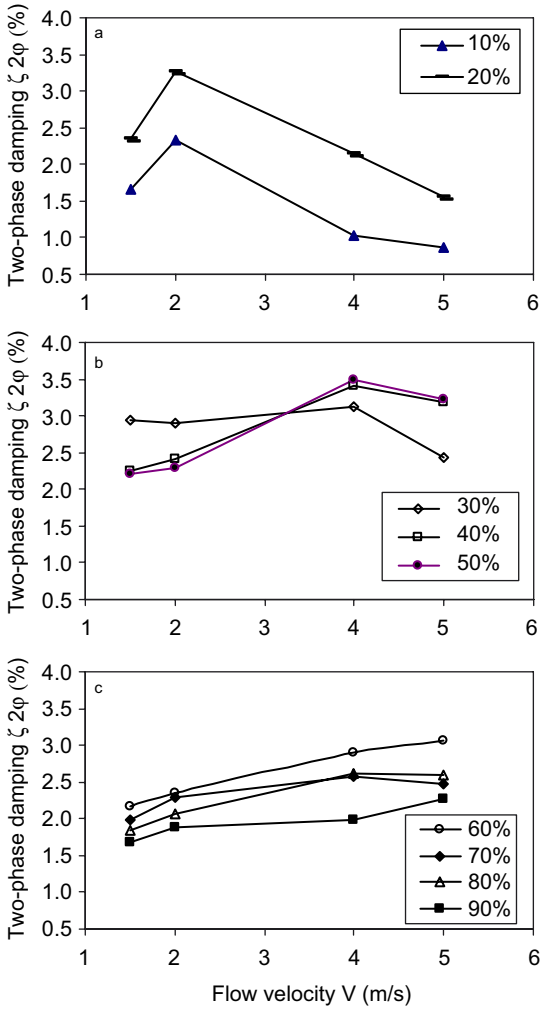

Fig. 8. Two-phase damping with respect to flow velocity: (a) low void fraction; (b) medium void fraction; and (c) high void fraction.

two-phase damping value and the respective void fraction for each flow velocity. The two-phase damping behavior seems to be divided in two categories. At lower velocities (Fig. 7(a) and (b)), the maximum damping occurs between 20% and 30% void fraction. The damping ratio decreases gradually at higher void fraction. At higher velocities (Fig. 7(c) and (d)), the maximum damping occurs at 50% void fraction, and a second, lower peak appears at 80% void fraction. Considering these very different peak locations with flow velocity, and the sharpness of the peaks, one may reasonably assume that some abrupt transformation in flow structure occurs that explain this behavior.

The same results are presented in terms of flow velocity in Fig. 8. It shows that for low void fractions (i.e. 10% and 20%), damping increases with flow velocity to a maximum at 2 m/s and then decreases with higher flow velocity.

At intermediate void fractions (30, 40 and 50%), the maximum is at a flow velocity around 4 m/s. At high void fractions (60–90%), there is no maximum; damping increases gradually with flow velocity from 1.5 to 5.0 m/s. Again, these trends suggest strong flow regime dependence as will be discussed in the next section.

4.3. Effect of flow regime

The prediction of flow regimes in vertical two-phase flows has been attempted by a number of researchers. Most of the experimental work has been done in small diameter tubes (i.e. 20–60 mm), containing upward low-pressure air–water flow or high-pressure steam-water flow. Hence, maps developed by Collier (1972) or by McQuillan and Whalley (1985) are used in the literature to provide insight into the possible flow regimes occurring in two-phase flows. However, the Taitel et al. (1980) approach was found to be more appropriate here because the models predicting flow pattern transition incorporate the effect of fluid properties and pipe sizes and thus are largely free of the limitations of the empirically based transitions maps or correlations.

The objective of Taitel et al. is to establish a physical explanation for each transition between flow regimes and to generate maps by simply using gas and liquid superficial velocities as coordinates ($U_{GS} = \varepsilon_g V$ and $U_{LS} = V(1-\varepsilon_g)$, respectively). Observations through the clear polymer tubes showed that most of our tests conditions lead to bubble, finely dispersed bubbles and churn flow structures. Indeed, although Fig. 9(a) shows five transition borders in the Taitel et al. map, Fig. 9(b) with the superimposed test points supports the visual observations indicating that the transitions occurred between the three afore mentioned flow regimes. For the finely dispersed bubble flow regime, the assumption is

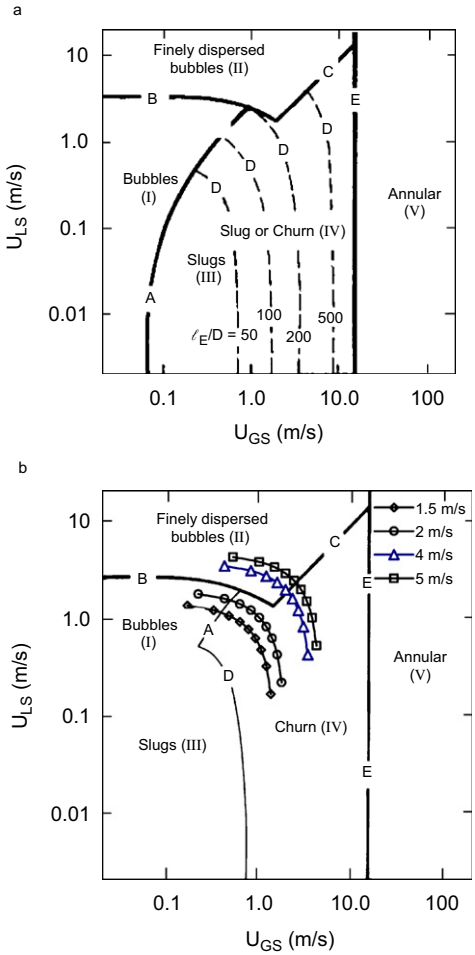

Fig. 9. Air–water flow pattern map (Taitel et al., 1980): (a) original map for $D_i = 25$ mm and (b) map fitted to test conditions with PVC test measurement points superimposed.

made that bubbles are small enough to remain spherical. Thus, bubbles bigger than the critical diameter d_c set by Brodkey (1967) belong to bubble flow,

$$d_c = \left[\frac{0.4\sigma}{(\rho_l - \rho_g)}\right]^{1/2}, \tag{7}$$

where σ is the surface tension, and ρ_l and ρ_g are the liquid and gaseous phase densities, respectively.

The maximum stable diameter $d_{\max}$ for a bubble evolving in turbulent liquid flow results from a balance between surface tension forces and those due to turbulent fluctuation. Hinze (1955), later confirmed by Sevik and Park (1973), established the following relationship:

$$d_{\max} = 1.14\left(\frac{\sigma}{\rho_l}\right)^{3/5}(\varepsilon)^{-2/5}, \tag{8}$$

where ε is the rate of energy dissipation per unit mass. It may be shown that the rate of energy dissipation is roughly related to velocity squared. Thus, a relationship between the maximum bubble diameter and flow velocity may be developed as shown in Fig. 10. Because turbulent forces lead to bubble break up, the bubble diameter decreases with flow velocity. The critical diameter governs the critical flow velocity V_c above which bubbles are assumed to be spherical and thus behave like rigid spheres. With Eq. (7), the critical bubble diameter may be estimated to be 1.7 mm for an air–water mixture. This corresponds to a critical flow velocity of 2.6 m/s following the relationship of Fig. 10. Hence, it supports the assumption that two different flow structures occur at low and at high velocities as discussed above. It also explains the difference between the two existing bubble regimes. Moreover, this may shed some light on the significant influence of flow regime on two-phase damping.

The transition between both the bubble and the finely dispersed bubble flow regimes toward churn flow is mainly based on the maximum allowable packing of the bubbles for both dominant and weak dispersion forces. In high velocity tests (i.e. above V_c) bubbles with spherical shape are modelled as evolving in a cubic lattice. Thus, the maximum void fraction before coalescence (geometrically speaking, when the bubble diameter equals the cube edge dimension) corresponds to the ratio of a bubble volume over its surrounding elementary cube volume, i.e. $\varepsilon_g = \pi/6$ as shown in Fig. 11. This void fraction is referred to as the "critical void fraction (ε_{gc})". Hence, Curve C in Fig. 9 relates U_{LS} and U_{GS} for $\varepsilon_g = \varepsilon_{gc} = 52\%$ above which dispersed bubbles can no longer be sustained.

At low velocities, bubble flow will collapse into churn flow at low void fractions as a result of the significant deformation and random flow path of larger bubbles. Some free motion of bubbles is assumed allowable without coalescence for spacing between bubbles up to approximately half their radius. This corresponds to a critical void fraction of approximately 25%. Thus, Curve A on Fig. 9 is generated using $\varepsilon_g = 25\%$, based on the rising velocity of relatively large bubbles as described by Harmathy (1960).

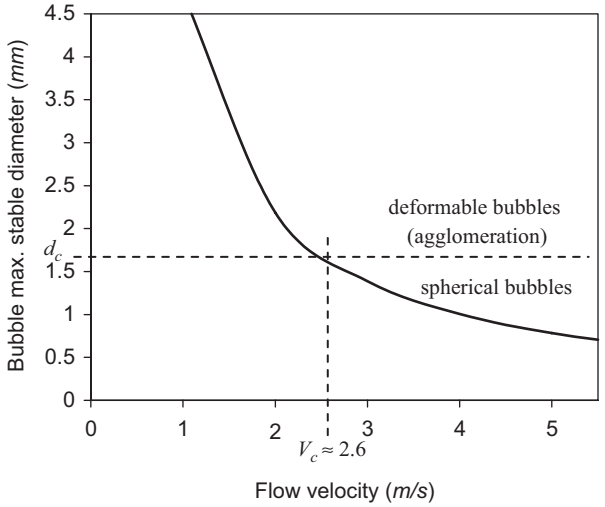

Fig. 10. Maximum bubbles diameter versus flow velocity, calculated using Eq. (8). Limit of deformable and spherical bubbles model from critical bubble diameter.

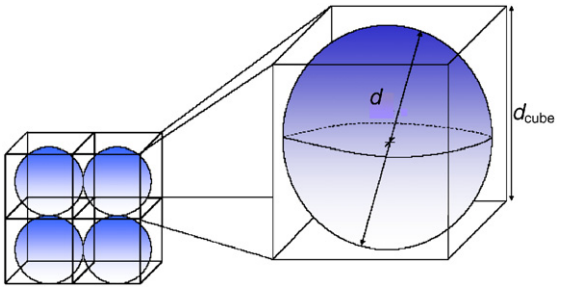

Fig. 11. Bubble flow model using a cubic elementary volume.

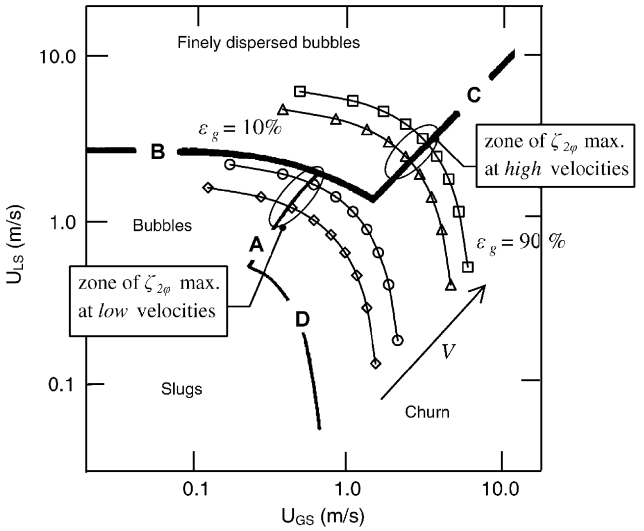

Fig. 12. Zoom of Taitel et al. map with superimposed test points showing transition at maximum damping ζ_{max} for flow velocities of 1.5 (◇), 2 (○), 4 (△) and 5 (□) m/s.

The use of the flow pattern map leads us to the conditions for which two-phase damping reaches a maximum as shown in Fig. 12. The maximum damping values correspond to the crossing of the transition Borders A and C, through which the flow passes from either a bubble regime or from finely dispersed bubbles towards a churn regime. The correlation between the flow pattern transition borders and the conditions shown in Fig. 7 for maximum damping is remarkably good. Moreover, the near-plateau in damping values, observed at higher void fractions in Fig. 7(a) and (b), corresponds to the churn flow regime which exists over a large range of void fractions at low flow velocities.

In addition, the interface surface area is largest near Borders A and C when the number and size of the bubbles are maximal just before the coalescence becomes significant, leading the flow structure to the churn flow regime. To verify the correlation between flow regime interfacial surface area and corresponding maximum damping values, further tests were conducted at constant superficial gas and liquid velocities as shown in Fig. 13. It shows that as long as the flow conditions stay close to the transition border near the dispersed bubble flow zone, the two-phase damping is highest.

5. Correlation with interphase surface area

Several authors, for instance Scriven and Hopley (1980), Hara (1988) and de Langre and Baj (2003), already considered some relationship between two-phase damping and the interfacial or interface surface area. The idea put forward is that the viscous behavior of the two-phase mixture is raised by confinement of the liquid phase due to the presence of the gas phase in the flow. Shear in the liquid phase is thus increased to allow for tube vibration. This theory

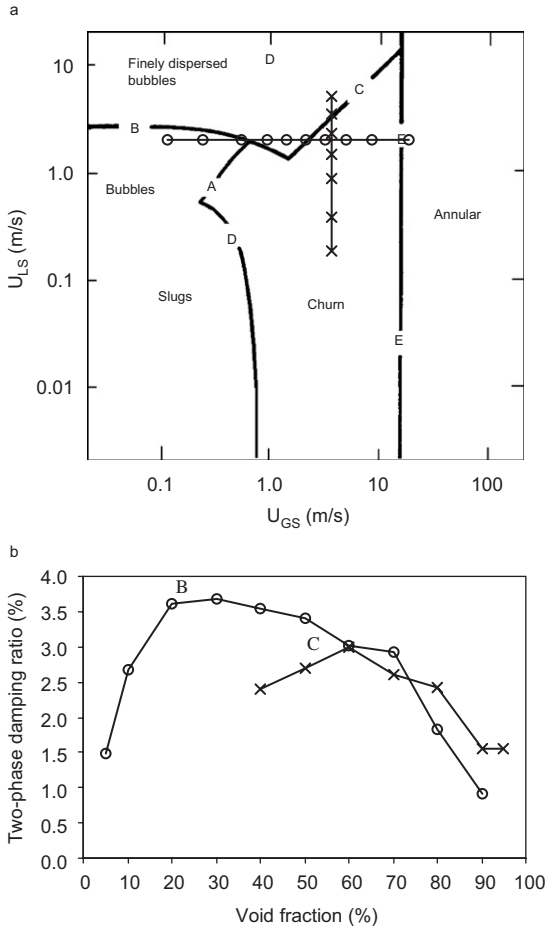

Fig. 13. Effect of flow regime on two-phase damping for superficial liquid velocity $U_{LS} = 2\,\text{m/s}$ (○) and superficial gas velocity $U_{GS} = 3.5\,\text{m/s}$ (X): (a) test points at constant superficial velocities superimposed on flow pattern map and (b) two-phase damping results showing location of transition borders B and C.

looks promising because the interface surface area appears proportional to the confinement of the liquid phase by the gas phase. However, the relative movement between the phases in the direction perpendicular to the flow, necessary to validate this theory, remains to be understood.

In external flow, the two-phase mixture, or most likely the gas phase because of its lower inertia, is displaced to accommodate the transverse motion of the vibrating tube. In internal flow, it is somewhat different since the two-phase mixture does not need to be displaced relative to the tube to allow for tube motion. In this case, the relative motion between phases is probably due to the much higher inertia of the liquid phase which tends to remain at rest while the gas phase accommodates most of the motion.

The interfacial surface area needs to be estimated to support the proposed theory. The estimation of the surface area must respect the characteristics of the flow regime and is achievable only by assuming bubbles to be rigid spheres. This assumption is valid only for high flow velocity as previously discussed. Nevertheless, an attempt was made to evaluate the behavior of the interface area at low flow velocity using the maximum stable diameter of large bubbles. However, it was not successful.

The aforementioned tests have a common characteristic: by increasing the void fraction the flow developed into an increasingly uniform dispersed bubbly structure. Then the bubbles coalesced in a nonlinear way up to 100% void fraction.

Before agglomeration and coalescence of the gas phase, the interfacial surface area depends on the number of bubbles and of their respective surface area. When the product of these two terms is highest, two-phase damping also reaches its maximum. The calculation of the interfacial surface area will be divided into two parts: bubble flow and churn flow. The bubble flow regime ($\varepsilon_g < \varepsilon_{gc}$) corresponds to the increasing part of the damping versus void fraction curve while the

churn flow regime ($\varepsilon_g > \varepsilon_{gc}$) relates to the decreasing part of the same curve. In bubbly flow, the surface, S, between the liquid phase and the bubbles has a total area of

$$S = S_b N, \tag{9}$$

where S_b is the surface area of one bubble simply defined as

$$S_b = 4\pi\left(\frac{d}{2}\right)^2, \tag{10}$$

where d is the bubble diameter. The total number of bubbles N may be deduced from the following ratio:

$$N = \frac{\text{Total volume of gas}}{\text{Volume of one bubble}}. \tag{11}$$

Hence, per unit of tube length, the foregoing ratio becomes

$$N = \frac{\varepsilon_g \pi (D/2)^2}{\frac{4}{3}\pi (d/2)^3}, \tag{12}$$

where D is the tube diameter. The combination of Eqs. (9)–(12) yields

$$S = \frac{3\varepsilon_g \pi D^2}{2d}. \tag{13}$$

Thus, the interface surface area in bubbly flow is inversely proportional to the bubble diameter.

5.1. Low void fractions

In dispersed bubble flow condition, the bubble diameter is limited by the critical diameter d_c expressed by Eq. (7). Thus, it is reasonable to assume that for the void fraction range $0 \leqslant \varepsilon_g \leqslant \varepsilon_{gc}$, the bubble diameter is a fraction of the critical diameter and is directly dependent on void fraction as follows:

$$d = d_c\left(\frac{\varepsilon_g}{\varepsilon_{gc}}\right)^{1/3}. \tag{14}$$

The exponent 1/3 is appropriate since the diameter of a sphere is related to the cubic root of its volume. As mentioned before, the value of ε_{gc} is 25% for low flow velocities, and 52% for high flow velocities. The value of the critical diameter d_c was previously calculated to be to 1.7 mm. Inserting the value of the bubble diameter, given in Eq. (14), into Eq. (13) and using the maximum surface $S_{\max}$ at the critical void fraction yields the interfacial surface area per unit length of tube for $0 \leqslant \varepsilon_g \leqslant \varepsilon_{gc}$:

$$\frac{S}{S_{\max}} = \left(\frac{\varepsilon_g}{\varepsilon_{gc}}\right)^{2/3}. \tag{15}$$

It should be noted that that the interface surface area depends on void fraction which, in turn, depends on the bubble diameter (d). For low flow velocities, the bubble diameter varies with flow velocity, as shown in Fig. 10. Thus, the calculated interface surface area is different for various flow velocities.

5.2. High void fractions

In the void fraction range $\varepsilon_{gc} \leqslant \varepsilon_g \leqslant 100$, the flow consists of bubbly flow sections separated by slugs. The interface surface area decreases with higher void fraction, as the slugs become larger, and the number of bubbles becomes lower. Bubble coalescence is a random and fairly complex phenomenon; thus, there is no known relationship between the interface surface area and the void fraction for slug flow at the present time. Therefore, a nonlinear interpolation is now assumed to relate the decreasing interfacial surface area S to the increasing void fraction ε_g:

$$S = S_{\max}\left(\frac{1-\varepsilon_g}{1-\varepsilon_{gc}}\right)^{1/3}, \tag{16}$$

where $S_{\max} = S_{(\varepsilon_g = \varepsilon_{gc})}$. This model ensures that $S = S_{\max}$ when $\varepsilon_g = \varepsilon_{gc}$, and $S = 0$ when $\varepsilon_g = 100\%$. The empirical exponent 1/3 was selected for a best fit with of the interface surface area with the damping ratio curves in the slug flow portion of the graphs ($\varepsilon_{gc} \leqslant \varepsilon_g$).

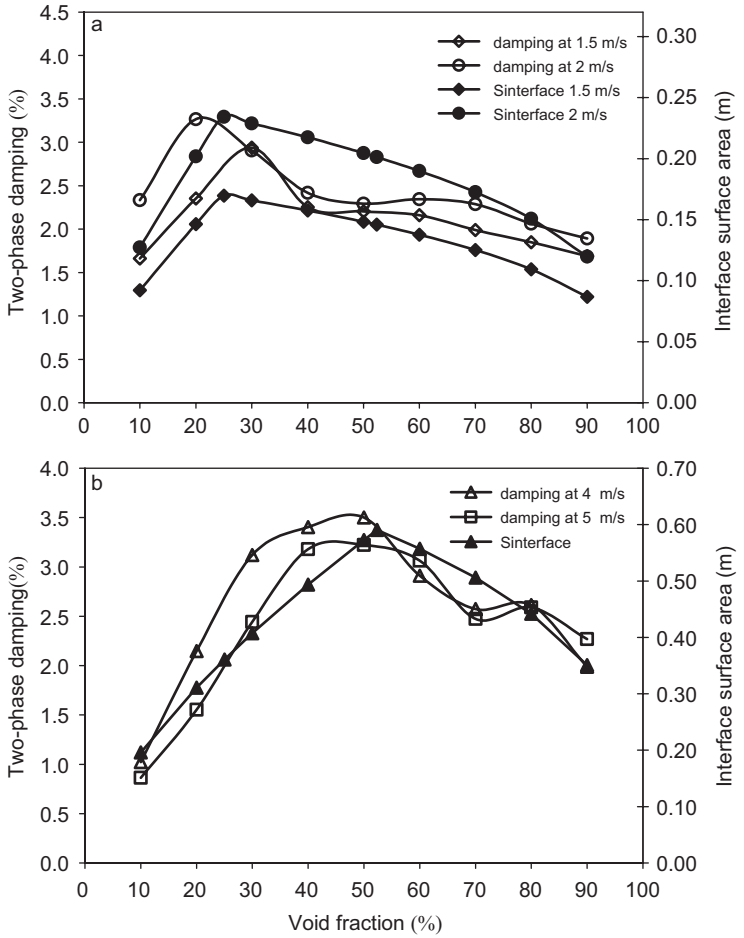

Fig. 14. Two-phase damping measured on PVC tube, and interface surface area calculated using Eqs. (15) and (16): (a) low flow velocities and (b) high flow velocities.

Again, it should be noted that turbulence at high flow velocities causes the bubbles to break up and to remain at the critical bubble diameter. It is assumed that the bubble size remains constant over the flow velocity range of interest. Therefore, the interface surface area is estimated to be the same at all considered flow velocities.

Eq. (16) complements Eq. (9) and it is now possible to evaluate the interface surface area over the entire range of void fractions, as shown in Fig. 14. The correlation between two-phase damping and the interface surface area is very good and it may be argued that it is a major parameter governing two-phase damping.

6. Conclusion

The purpose of this study is to understand the parameters that govern damping in internal two-phase flows. Tests on three tubes of similar diameters but of different materials were conducted. The results show the following:

(i) At high flow velocities, the two-phase damping measurements are in good agreement with those generally reported in the literature. Two-phase damping increases with increasing void fraction, reaching a maximum at roughly 50% void fraction beyond which it decreases gradually.
(ii) At lower velocity, the maximum damping occurs at lower void fractions (i.e. around 25%).
(iii) The maximum damping ratio, which is roughly 3%, is similar for both high and low flow velocities.

(iv) Two-phase damping is found to be largely governed by flow regime, the highest damping values occurring in the bubble flow regime near the transition zone.

(v) There is a direct correlation between two-phase damping and the interface surface area, estimated assuming rigid spherical bubbles. It appears that viscous dissipation mechanisms govern the additional component of damping due to two-phase flow.

Acknowledgements

This work was supported by the Natural Sciences and Engineering Research Council of Canada (NSERC) though the BWC/AECL/NSERC Industrial Research Chair in Fluid–Structure Interaction.

References

Brodkey, R.S., 1967. The Phenomena of Fluid Motions. Addison-Wesley Press, Reading, MA.

Carlucci, L.N., 1980. Damping and hydrodynamic mass of a cylinder in simulated two-phase flow. Journal of Mechanical Design 102, 597–602.

Carlucci, L.N., Brown, J.D., 1983. Experimental studies of damping and hydrodynamic mass of a cylinder in confined two-phase flow. ASME Journal of Vibration, Acoustics, Stress, and Reliability in Design 105, 83–89.

Collier, J.G., 1972. Convective Boiling and Condensation, first ed. McGraw-Hill, London.

de Langre, E., Baj, F., 2003. Scaling of damping induced by bubbly flow across tubes. Journal of Fluids and Structures 17, 351–364.

Hara, F., 1988. Two-phase fluid damping in a vibrating circular structure. In: Proceedings of the ASME PVP Conference, PVP-vol. 133, Pittsburgh, PA, USA, ASME, New York, pp. 1–8.

Harmathy, T.Z., 1960. Velocity of large drops and bubbles in media of infinite or restricted extent. AIChE Journal 6, 281–288.

Hinze, J.O., 1955. Fundamental of the hydrodynamics mechanism of splitting in dispersion processes. AIChE Journal 1, 289–295.

McQuillan, K.W., Whalley, P.B., 1985. Flow patterns in vertical two-phase flow. Journal of Multiphase Flow 11 (2), 161–175.

Païdoussis, M.P., 1998. Fluid–Structure Interactions: Slender Structures and Axial Flow, vol. 1. Academic Press, London, UK.

Pettigrew, M.J., Knowles, G.D., 1997. Some aspects of heat exchanger tubes in two-phase mixtures. Journal of Fluids and Structures 11, 929–945.

Pettigrew, M.J., Taylor, C.E., 1997. Damping of heat exchanger tubes in two-phase flow. In: Fluid–Structure Interactions, Aeroelasticity, Flow-Induced Vibration and Noise, AD-vol. 53-2, Dallas, Texas, pp. 407–418.

Pettigrew, M.J., Taylor, C.E., 2004. Damping of heat exchanger tubes in two-phase flow: review and design guidelines. ASME Journal of Pressure Vessel Technology 126, 523–533.

Pettigrew, M.J., Taylor, C.E., Kim, B.S., 2001. The effects of bundle geometry on heat exchanger tube vibration in two-phase flow. ASME Journal of Pressure Vessel Technology 123, 414–420.

Roumy, R., 1969. Structure des écoulememts diphasiques eau-air. Etude de la fraction de vide moyenne et des configurations d'écoulement, CEA-R-3892. Commissariat à l'Energie Atomique, France.

Scriven, A.H., Hopley, C.E., 1980. The effect of an internal two-phase flow on the damping characteristics of a vibrating tube. CERL—Strathclyde University, Glasgow.

Sevik, M., Park, S.H., 1973. The splitting of drops and bubbles by turbulent fluid flow. ASME Journal of Fluids Engineering 95, 53–60.

Taitel, Y., Bornea, D., Dukler, A.E., 1980. Modelling flow pattern transitions for steady upward gas–liquid in vertical tubes. AIChE Journal 26, 345–354.